

Flexural ductility of reinforced and prestressed concrete sections with corrugated steel webs

X.C. Chen¹, F.T.K. Au^{*1}, Z.Z. Bai^{1,2}, Z.H. Li^{1,3} and R.J. Jiang^{1,3}

¹Department of Civil Engineering, The University of Hong Kong, Hong Kong, China

²Department of Bridge Engineering, Tongji University, Shanghai, China

³Research Center, Shenzhen Municipal Engineering Design and Research Institute, Shenzhen, China

(Received June 10, 2015, Revised October 19, 2015, Accepted October 22, 2015)

Abstract. Prestressed concrete bridges with corrugated steel webs have emerged as one of the promising bridge forms. This structural form provides excellent structural efficiency with the concrete flanges primarily taking bending and the corrugated steel webs primarily taking shear. In the design of this type of bridges, the flexural ductility and deformability as well as strength need to be carefully examined. Evaluation of these safety-related attributes requires the estimation of full-range behaviour. In this study, the full-range behaviour of beam sections with corrugated steel webs is evaluated by means of a nonlinear analytical method which uses the actual stress-strain curves of the materials and considers the path-dependence of materials. In view of the different behaviour of components and the large shear deformation of corrugated steel webs with negligible longitudinal stiffness, the assumption that plane sections remain plane may no longer be valid. The interaction between shear deformation and local bending of flanges may cause additional stress in flanges, which is considered in this study. The numerical results obtained are compared with experimental results for verification. A parametric study is undertaken to clarify the effects of various parameters on ductility, deformability and strength.

Keywords: corrugated steel web; ductility and deformability; flexural strength; partially prestressed concrete; reinforced concrete

1. Introduction

The concrete bridge with corrugated steel webs is a structural form in which the steel webs mainly resist shear force and the concrete flanges mainly resist bending moment. This form of bridge has some remarkable advantages such as lightness, high shear buckling strength of steel webs, efficient prestressing of concrete and easy maintenance. In 1986, the first bridge of this type, Cognac Bridge, was built in France (Cheyrezy and Combault 1990). Because of the successful application and its remarkable advantages, this type of bridges becomes popular worldwide, especially in Japan and China. Hereafter in this paper, this form of bridge is assumed unless otherwise stated.

A typical cross section of the bridge is shown in Fig. 1(a), where t_u and t_l are the depths of the

*Corresponding author, Professor, E-mail: francis.au@hku.hk

upper and lower flanges respectively; b_u and b_l are the widths of the upper and lower flanges respectively; h_w is the height of the steel web; and h is the distance between the centroidal axes of flanges. Fig. 1(b) shows typical forms of corrugated web (trapezoidal and sinusoidal) where s denotes the developed length of a half corrugation; s_0 denotes its projected length; r denotes the rise of corrugation; and θ denotes the trough angle. The corrugated steel web is usually analysed by the theory of orthotropic plates. The equivalent orthotropic shear modulus G_e of the corrugated web is given by $G_e=(s_0/s)G_w$, where G_w is the shear modulus of steel (Briassoulis, 1986, Samanta and Mukhopadhyay, 1999).

In view of the different behaviour of components and the large shear deformation of corrugated webs with negligible longitudinal stiffness, the assumption that plane sections remain plane may no longer be valid for this type of bridges. The behaviour of the bridge as shown in Fig. 2(a) is similar to that of a sandwich beam with thick facings as shown in Fig. 2(b). The flexural rigidities of both the corrugated steel webs of the bridge and the core of the sandwich beam are negligible. Chen *et al.* (2015b) proposed an extended sandwich beam model to predict the elastic behaviour taking into account the effects of diaphragm and interaction between shear deformation and local bending of concrete flanges. The proposed model was verified by three-dimensional finite element model and tests.

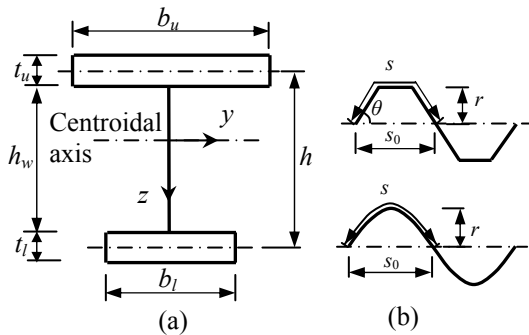


Fig. 1 A cross section of bridge and typical web corrugations: (a) a simplified section; and (b) typical web corrugations

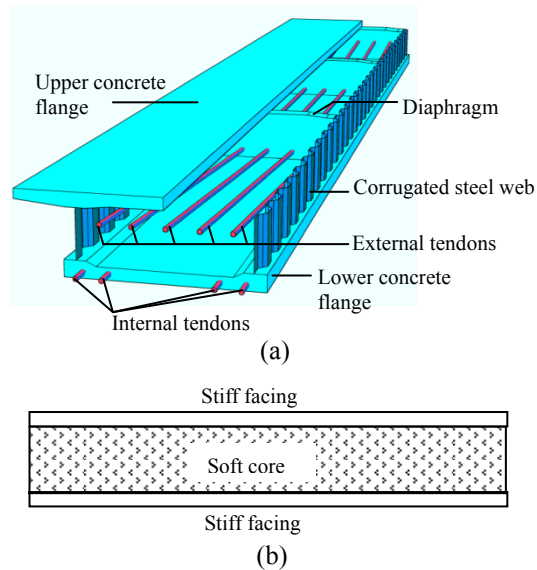


Fig. 2 Comparison of a bridge and a sandwich beam with thick faces: (a) A bridge; and (b) a sandwich beam with thick faces

In the design of this type of bridges, especially those with flanges made of high-strength concrete and those with the requirement of seismic resistance, the flexural ductility and deformability as well as strength need to be carefully examined. Evaluation of these safety-related attributes requires the reliable estimation of full-range behaviour that encompasses the service and failure behaviour. Thompson and Park (1980), Naaman *et al.* (1986), Cohn and Riva (1991)

conducted the theoretical moment-curvature analysis of conventional prestressed concrete sections with bonded prestressing steel. Carreira and Chu (1986) presented a general nonlinear method to compute the moment-curvature relationship of conventional reinforced concrete (RC) members. A numerical method for the moment-curvature analysis of RC beams, which takes into account the nonlinear stress-strain relationship as well as stress-path dependence of the constitutive materials, has been developed and applied to conventional rectangular beams (Ho *et al.* 2003, Bai and Au 2013) and flanged beams (Kwan and Au 2004). Many other researchers also studied the nonlinear behaviour of conventional sections, e.g., Whitehead and Ibell (2004), Havaei and Keramati (2011), Barros and Martins (2012), Pandey (2013), Lee (2013), Chen *et al.* (2015a), but relatively little has been done on the present type of bridges.

In this study, the full-range behaviour of reinforced concrete and partially prestressed concrete (PPC) sections with corrugated steel webs is evaluated by means of a nonlinear numerical method which uses the actual stress-strain curves of the materials and considers their stress-path dependence. An extensive parametric study is undertaken to clarify the effects of various parameters such as the section shape, grade of concrete, steel content, partial prestressing ratio, prestressing force ratio, *etc.* on the ductility, deformability and strength of the bridge section. The numerical results will also be examined in the light of available experimental results.

2. Method of analysis

2.1 Constitutive models of materials

The stress-strain relationship for concrete in compression as proposed by Attard and Setunge (1996) and Attard and Stewart (1998), which applies to a broad range of in-situ concrete compressive strength from 20 to 130 MPa, is adopted in the study. The stress-strain relationship for concrete in tension is assumed to be linear with a slope equal to the elastic modulus in compression at zero stress. The tensile strength of concrete is determined according to Carreira and Chu (1986). To consider the post-cracking resistance in tension, the model proposed by Guo and Zhang (1987) is adopted. To consider strain reversal of concrete, it is assumed that the unloading path of the stress-strain curve is linear and has the slope proposed by Elmorsori *et al.* (1998). The typical loading and unloading curves of concrete adopted are shown in Fig. 3(a), in which E_c is the initial modulus of elasticity of concrete; f_{co} is peak compressive stress (in-situ uniaxial compressive strength) of concrete, ε_{co} is the strain at peak stress of concrete; f_t is the tensile strength of concrete; and ε_t is the tensile strain at tensile strength of concrete.

The stress-strain curve recommended by Mander *et al.* (1984) is used for the non-prestressed reinforcement and corrugated steel web. The curve comprises an initial linearly elastic portion, a flat yield plateau and a nonlinear strain hardening portion. To cater for strain reversal, it is assumed that the unloading path of the stress-strain curve is linear and has the same slope as the initial elastic portion. The typical loading and unloading curves of non-prestressed steel applied are shown in Fig. 3(b), in which E_s is the modulus of elasticity; f_y is the yield strength; f_u is the ultimate strength; ε_{sh} and E_{sh} are the strain and tangent modulus when strain hardening just begins. Strain hardening in the compression reinforcement is not considered as local buckling normally occurs earlier than strain hardening at inelastic stage.

The stress-strain formula for prestressing steel proposed by Menegotto and Pinto (1973) with empirical parameters recommended by Naaman (1985) is adopted. It is assumed that the unloading

path of the stress-strain curve is linear and has the same slope as the initial elastic modulus. The loading and unloading curves of the prestressing steel adopted are shown in Fig. 3(c), in which E_p is the modulus of elasticity of prestressing steel; f_{pu} and ϵ_{pu} are the ultimate stress and strain respectively of prestressing steel; and f_{py} and ϵ_{py} are the “yield” stress taken as $0.85 f_{pu}$ and the corresponding strain of prestressing steel respectively.

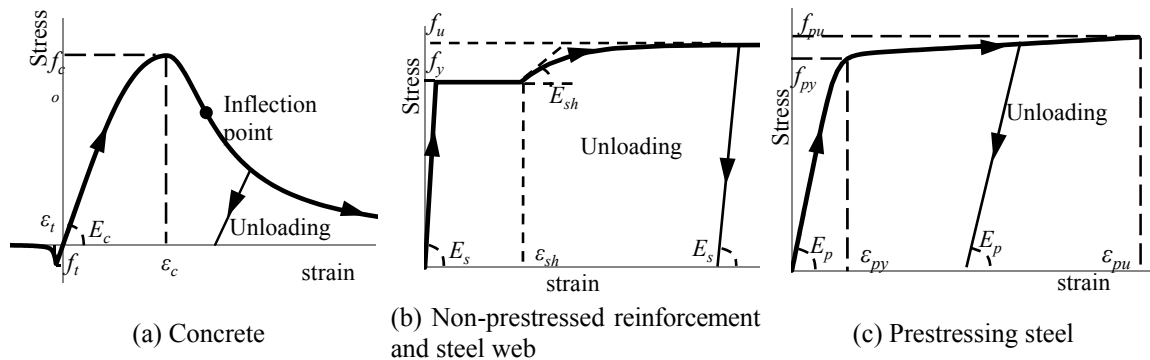


Fig. 3 Stress-strain relationship of materials with stress path dependence

2.2 Method of analysis

The assumptions adopted are: (a) the stress-strain relationships of concrete, non-prestressed and prestressing steel are as given by the constitutive models adopted; (b) the non-prestressed reinforcing steel and internal prestressing steel are perfectly bonded with surrounding concrete; (c) the corrugated steel webs are perfectly bonded with concrete flanges; (d) the flexural rigidity of corrugated steel webs is negligible; and (e) the shear deformation in concrete flanges is negligible. The interaction between shear deformation and local bending of concrete flanges may cause significant stress concentration in concrete flanges in the vicinity of the diaphragm and point load. Except for these local regions, the interaction effects are normally insignificant and therefore the assumption of linear normal strain distribution over section depth is roughly valid over there as the conventional beam sections. Hence, the assumption of linear strain distribution is adopted in Section 3 for the general cases. The interaction effects are discussed in Section 4 where a secondary curvature is introduced to account for these effects.

A computer programme based on the numerical approach of Ho *et al.* (2003) is developed with proper modification for such bridges. In this study, apart from ordinary non-prestressed reinforcement, prestressing steel has also been incorporated so that the computer programme can cover both RC and PPC sections. For a section with negligible interaction effects, in each iteration cycle, the strain variation is determined assuming linear strain distribution over the section depth according to the prescribed curvature ϕ as shown in Fig. 4(a), and the stresses in the concrete and steel components are evaluated from their respective constitutive models accordingly. When the interaction effects need to be considered especially in the vicinity of the point load or diaphragm, in addition to the primary curvature ϕ_1 that is based on the average axial strain of each of the concrete flanges, the secondary local curvature ϕ_2 in concrete flanges as shown in Fig. 4(b) is needed to account for the additional curvature due to interaction effect. An iterative process is

adopted such that the primary curvature ϕ_1 is prescribed incrementally and the secondary local curvature ϕ_2 is determined accordingly from sectional and structural equilibrium. The total curvature ϕ is the sum of the primary curvature ϕ_1 and the secondary local curvature ϕ_2 , i.e., $\phi = \phi_1 + \phi_2$. Axial equilibrium is used to determine the neutral axis depth, d_n , after which the resisting moment is calculated. This iterative process is repeated until sufficient length of the full-range moment-curvature curve has been obtained.



Fig. 4 Strain distribution over section depth

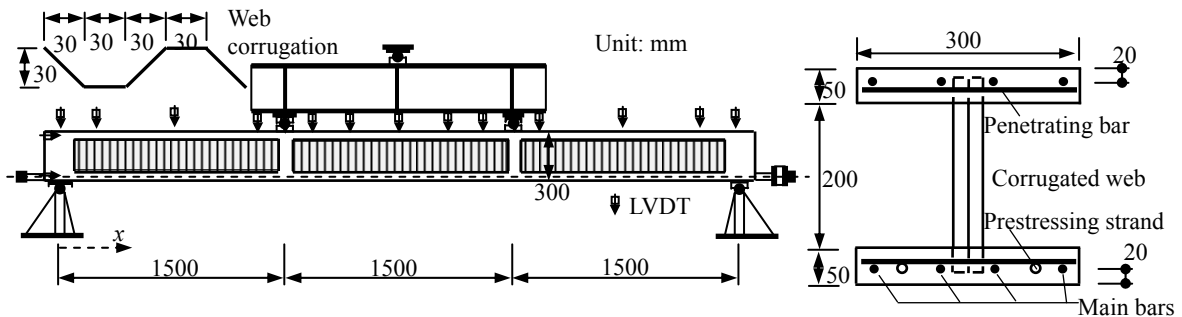


Fig. 5 Configuration of specimen P-1 tested

2.3 Verification of the numerical model

The numerical model developed is verified by experiments. A PPC beam specimen with a 5 mm thick single corrugated steel web, denoted by “P-1”, was fabricated for testing over a span of 4500 mm as shown in Fig. 5. The specimen was 4700 mm in length, 300 mm in both depth and breadth, and pre-tensioned by two prestressing steel strands located in the lower flange at 20 mm above the soffit. Embedment connections were provided between the concrete flanges and corrugated steel web. To prevent or delay bond-slip between the prestressing strands and their surrounding concrete, the end anchorages for prestressing were retained.

The effective prestressing force of specimen was 186 kN. The specimen was simply supported and tested by third-point loading by displacement control as shown in Fig. 6. Linear variable differential transformers (LVDTs) were used to measure displacements during the loading test.

Table 1 Properties of materials from tests (unit: MPa)

	Concrete	Steel reinforcement	Prestressing strand	Steel web
Initial Young's modulus	30962	192277	206780	196056
Yield strength	-	559	-	267
Ultimate strength	67.7 (cube strength)	672	2008	399



Fig. 6 Test setup of specimen P-1

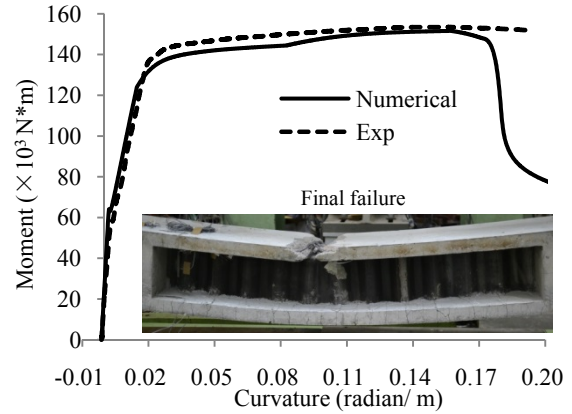


Fig. 7 Moment-curvature curve for mid-span section of specimen P-1

Routine tests of the materials were carried out to identify the quality of materials and the results are tabulated in Table 1.

The moment-curvature curve for the mid-span section obtained by the numerical model is compared with experimental result as shown in Fig. 7, in which good agreement is observed. Due to the relatively soft local aggregates used in Hong Kong, the initial Young's modulus of concrete is relatively lower. Hence, the measured initial Young's modulus of concrete is adopted in the numerical model instead of the value suggested by the concrete model of Attard and Setunge (1996). The ductility factors μ from experimental and numerical results are 9.816 and 9.315 respectively in accordance with the method proposed by Park (1988) and Au *et al.* (2011), i.e.

$$\mu = \phi_u / \phi_y \quad (1)$$

where ϕ_u and ϕ_y are the equivalent ultimate curvature and yield curvature respectively.

3. Nonlinear sectional analysis

3.1 Full-range behaviour of typical sections

3.1.1 Sections analysed

To evaluate the ductility of the section with corrugated steel webs, its nonlinear behaviour is compared with conventional box girder and rectangular concrete sections with the same overall dimensions. Four PC or PPC sections are analysed in this study as shown in Fig. 8. Section I is a section with corrugated steel webs. Sections II and III are conventional box girder sections with

total web widths b_w of 900 mm and 1800 mm respectively. Section IV is a rectangular section. These four sections have the same overall dimension of depth $H=1800$ mm and breadth $b_u=6000$ mm. The lower flanges of Sections I - III have the same width of $b_f=4000$ mm. The upper and lower flanges of Sections I - III are 350 mm thick. The centroids of both the non-prestressed reinforcement and prestressing tendons are 175mm above the soffit.

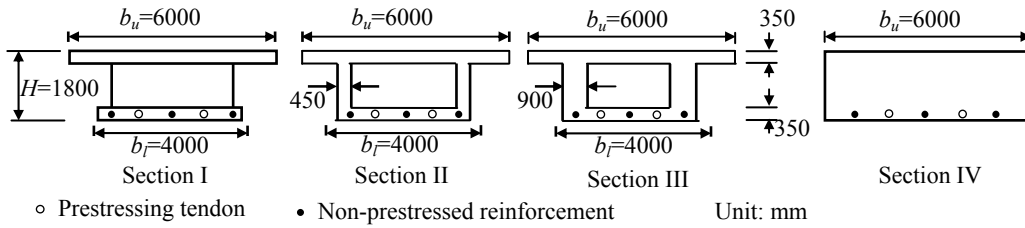


Fig. 8 Typical bridge sections analysed

To improve the behaviour under service condition, prestressing steel tendons may be provided in addition to the non-prestressed reinforcement. The partial prestressing ratio, PPR, is defined as

$$PPR = (A_p f_{py}) / (A_p f_{py} + A_s f_y) \quad (2)$$

where A_p is the cross-sectional area of prestressing steel; and A_s is the area of non-prestressed tension reinforcing steel. The equivalent tension steel area A_{se} is defined here as

$$A_{se} = (A_p f_{py} + A_s f_y) / f_y \quad (3)$$

The equivalent tension steel area at which balanced failure (or simultaneous failure in tensile yielding of steel and crushing of concrete in compression) occurs is taken as the equivalent balanced steel area and denoted by $A_{se,b}$. The equivalent tension to balanced steel ratio is defined as $A_{se}/A_{se,b}$ and may be considered as a measure of the degree of the section being under- or over-reinforced.

As pointed out by Au *et al.* (2011), the traditional definition of ductility factor of prestressed or partially prestressed sections may give misleading results in some cases and deformability may be a more reliable indicator of safety. The deformability indicator is proposed as $\phi_u H$, which can be evaluated as a simple function of the neutral axis depth ratio $d_{n,peak}/d$, where $d_{n,peak}$ is the neutral axis depth at peak resisting moment; and d is the effective depth to centroid of tension steel. Limiting the ratio $d_{n,peak}/d$ is a popular method in design codes for flexural ductility design of RC and PPC beams.

3.1.2 Complete moment-curvature curves

For example, the in-situ concrete compression strength f_{co} , the yield strength f_y of non-prestressed tension reinforcement, and the ultimate strength f_{pu} of prestressing steel are taken as 50 MPa, 500 MPa, and 1860 MPa respectively. The Young's moduli of non-prestressed and prestressing steel are assumed to be 200 GPa. The prestressing force ratio f_{pe}/f_{pu} is taken as 0.7, where f_{pe} is the effective prestress. The strain hardening of non-prestressed reinforcement is

neglected here for simplicity.

The same amount of equivalent area of tension steel $A_{se}=0.15 \text{ m}^2$ is provided in all the sections analysed. The parameters are so chosen that the tensile stress at transfer of the concrete fibre does not exceed the tensile strength at transfer taking into account the bending moment caused by the self-weight of bridge. For example, the self-weight is calculated assuming the section analysed is at the mid-span of a simply supported bridge with a span of 30 m. The densities of concrete flanges and steel web are assumed to be 25 kN/m^3 and 78 kN/m^3 respectively.

The complete moment-curvature curves of Sections I - IV in Fig. 9 show that, when the same amount of equivalent tension steel area is used, the moment-curvature curves for these four sections display similar peak moments irrespective of PPR, as all four sections are under-reinforced.

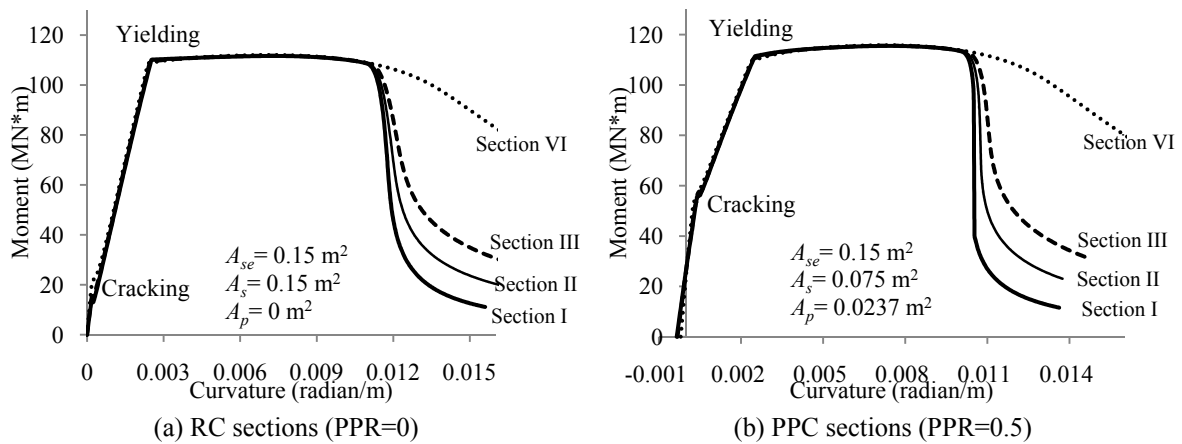


Fig. 9 Complete moment-curvature curves of sections with same overall dimensions and amount of equivalent tension steel area

During the elastic and cracked elastic stages, the moment-curvature curves of all four sections follow almost the same bi-linear path. After the yielding of non-prestressed reinforcement, they develop a relatively flat yield plateau before the resisting moments drop significantly. The moment-curvature curve of Section I with corrugated steel webs drops very sharply. Sections II and III also display a relatively sharp drop in the moment-curvature curves but slightly less rapid compared to Section I. Thus Sections II and III have slightly higher ductility factors than Section I. As the post-peak branch of rectangular Section IV is much smoother and without a sudden drop, its ductility is the highest. It is evident that the concrete in web of Sections II and III contributes little to the peak resisting moment, but it does contribute to the residual resisting moment at the post-peak stage, thus benefitting their ductility. Hence Section III with thicker concrete webs has slightly higher ductility. As pointed out by Kwan and Au (2004), the concrete near the section centre contributes significantly to the flexural ductility of the beam section. At the post-peak stage, when the resisting moment decreases after reaching its peak value, the concrete near the extreme compression fibre is gradually losing its strength and the neutral axis of the section moves towards the tension reinforcement. Consequently at the post-peak stage, the concrete near the section centre develops much higher compressive stresses than before and contributes significantly to the

residual moment resisting capacity of the section. Therefore, a rectangular section having the most concrete near the centre is the most ductile. In other words, although a flanged section has higher structural efficiency in terms of flexural strength, it has lower flexural ductility. Because of the negligible flexural rigidity of the corrugated steel webs of Section I, it can be taken as an extreme case of flanged section with no concrete web. Actually Section IV being wasteful of materials is unrealistic for practical use in bridges. The box girder versions of Sections I - III all provide similar flexural strength and ductility. Comparing Figs. 9(a) and (b), the applied prestressing force has also delayed the cracking of the PPC sections compared with the RC sections.

The effects of prestressing force ratio on the moment-curvature curve of Section I with corrugated steel webs are shown in Fig. 10. The ultimate curvatures are almost the same for cases with different prestressing force ratios f_{pe}/f_{pu} therefore giving almost the same deformability indicators. However, the higher the prestressing force ratio is, the earlier the moment reaches the peak value, and hence the lower the yield curvature and the higher the ductility. As the value of PPR increases from zero to unity, the section gradually changes from an RC section to a fully prestressed section. The moment-curvature curves of Section I with corrugated steel webs for different values of PPR in Fig. 11 show that, the higher the PPR is, the later the moment reaches the peak value and the faster it drops, which cause the lower ductility and deformability. At the same equivalent tension steel area A_{se} , the peak moments are almost same irrespective of the prestressing force ratio and PPR. Similar conclusions can be drawn for Sections II - IV. For convenience of comparison, the curvature at the beginning of loading is taken as zero in Figs. 10 and 11.

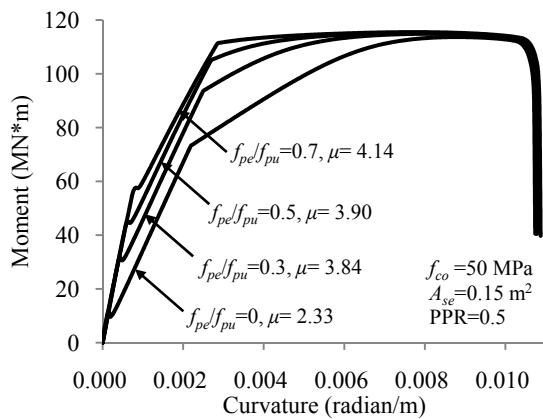


Fig. 10 Complete moment-curvature curves of Section I with different prestressing force ratios

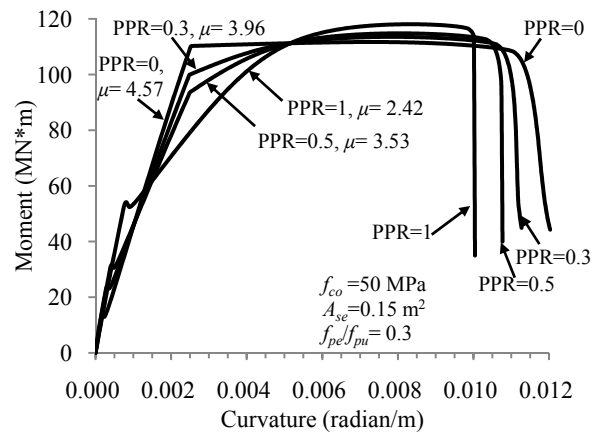


Fig. 11 Complete moment-curvature curves of Section I with different PPR

3.2 Flexural ductility and deformability of typical sections

Although Fig. 9 shows that, at the same overall dimensions and equivalent tension steel area, the sections with corrugated steel webs have lower ductility factor and deformability indicators, a fair comparison can only be carried out by considering the equivalent tension to balanced steel ratio $A_{se}/A_{se,b}$ in view of the large differences in concrete area. In the comparison, the overall

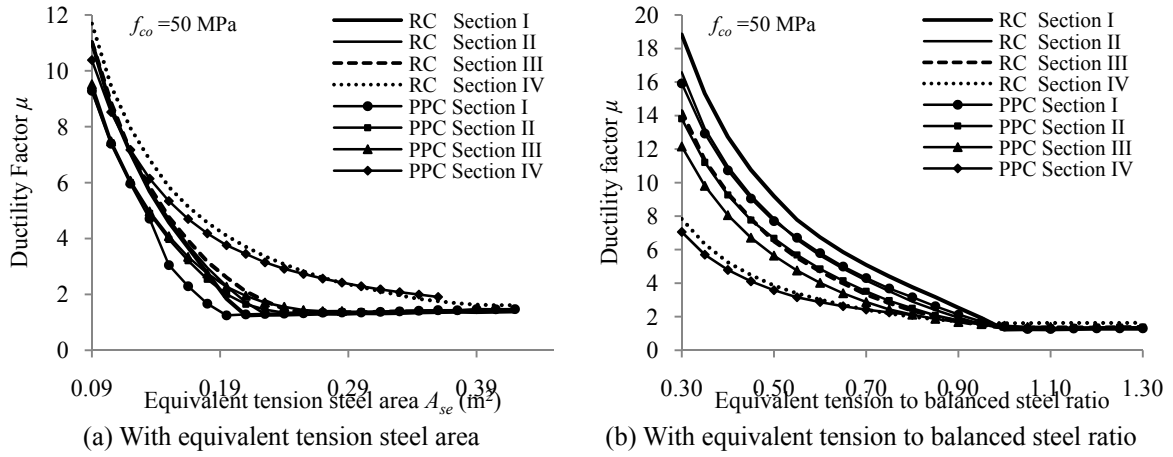


Fig. 12 Variation of ductility factor of sections analysed

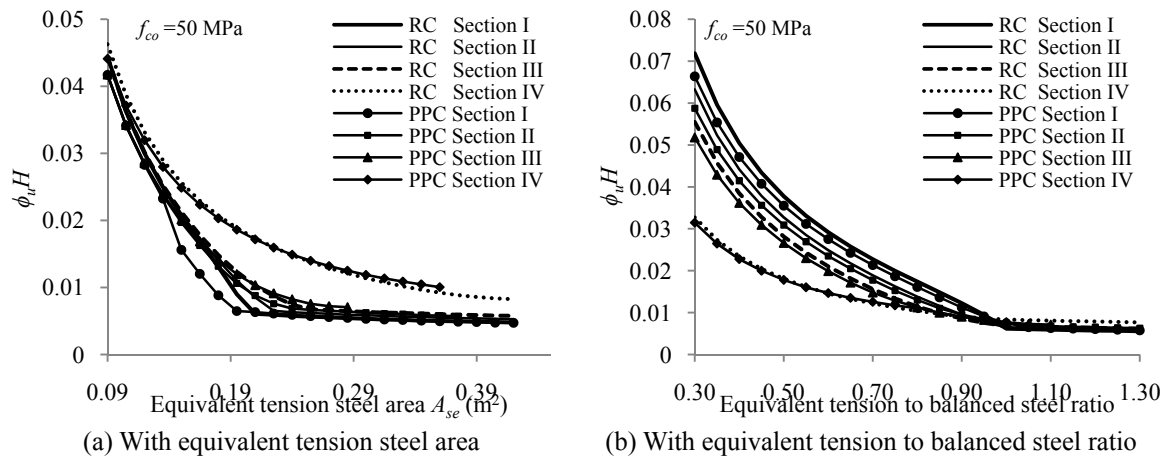


Fig. 13 Variation of deformability indicator of sections analysed

dimensions and material properties of the sections analysed are kept unchanged. Both the prestressing force ratio f_{pe}/f_{pu} and partial prestressing ratio PPR are assumed to be 0.5.

Figs. 12(a) and (b) show the variation of the ductility factor μ with the equivalent tension steel area A_{se} and the equivalent tension to balanced steel ratio $A_{se}/A_{se,b}$, respectively, for RC and PPC versions of Sections I-IV. With the increase of the equivalent tension steel area A_{se} or the equivalent tension to balanced steel ratio $A_{se}/A_{se,b}$, the ductility factor decreases. At the same equivalent tension steel area A_{se} , generally Section I with corrugated steel webs has the lowest ductility factor, followed by Sections II-III of conventional concrete box girder construction, while Section IV of solid construction has the highest ductility factor, because Section I is relatively heavily reinforced as its equivalent balanced steel area is the smallest. However, at the same equivalent tension to balanced steel ratio $A_{se}/A_{se,b}$ below 1.0, Section I with corrugated steel webs has the highest ductility factor, followed by Sections II and III of conventional concrete box girder construction, and then Section IV of solid construction. When the equivalent tension to balanced steel ratio exceeds 1.0, the ductility factors become stable with negligible difference.

Figs. 13(a) and (b) show the variation of the deformability indicator $\phi_u H$ with the equivalent tension steel area A_{se} and the equivalent tension to balanced steel ratio $A_{se}/A_{se,b}$, respectively, for the sections analysed. Regarding the variation of deformability indicator $\phi_u H$, conclusions similar to those for the ductility factor μ can be drawn. At the same tension steel area, generally Section I with corrugated steel webs has the lowest deformability indicator $\phi_u H$, while at the same equivalent tension to balanced steel ratio $A_{se}/A_{se,b}$ below 1.0, Section I with corrugated steel webs has the highest deformability indicator $\phi_u H$.

Figs. 14(a) and (b) show the effects of the neutral axis depth ratio $d_{n,peak}/d$ on the ductility factor μ and deformability indicator $\phi_u H$ respectively for RC and PPC versions of Sections I-IV. With the exception of the solid sections, the curves tend to come close to one another, and this phenomenon is more obvious for deformability indicator. Therefore, the deformability indicator $\phi_u H$ can be evaluated as a simple function of the ratio $d_{n,peak}/d$ better than the ductility factor μ , whether the concrete sections are reinforced or partially prestressed. In other words, it is possible to develop empirical formulae to predict the ductility and deformability based on the neutral axis depth ratio at peak resisting moment.

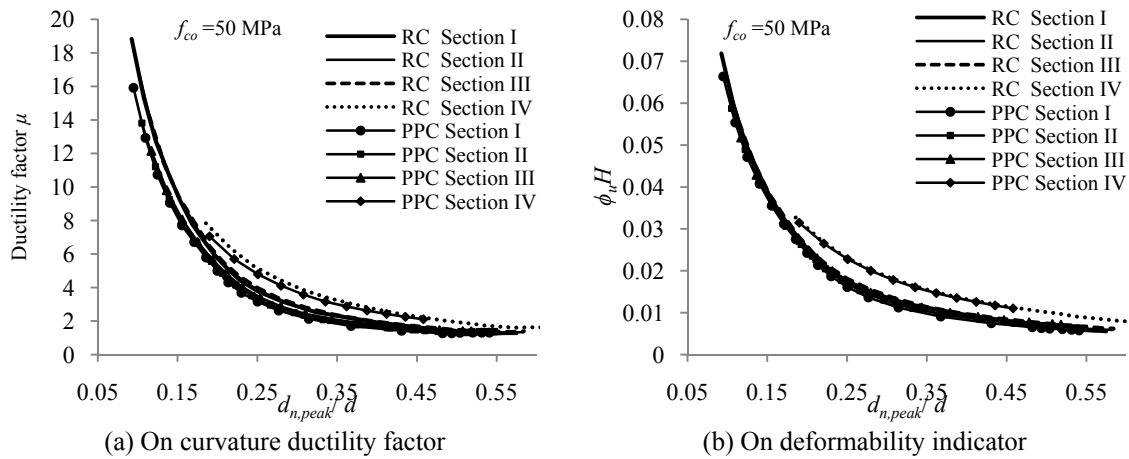


Fig. 14 Effects of $d_{n,peak}/d$ ratio of sections analysed

3.3 Flexural strength - ductility and flexural strength - deformability performance

The overall dimensions and material properties of the sections analysed are kept unchanged. Both the prestressing force ratio f_{pe}/f_{pu} and partial prestressing ratio PPR are assumed to be 0.5. The equivalent tension to balanced steel ratio $A_{se}/A_{se,b}$ is varied from 0.3 to 1.3 at an interval of 0.05. The peak moment, ductility factor and deformability indicator are calculated for each given equivalent tension to balanced steel ratio.

Figs. 15 and 16 show the flexural strength - ductility and flexural strength - deformability performance, respectively, of sections having the same overall dimensions but different section shapes. The flexural strength is expressed in terms of $M_p/b_u d^2$ so as to account for the size effects and facilitate convenient comparison. In this manner of comparison, the flexural strength - ductility and flexural strength - deformability curves of the sections with corrugated steel webs are lower than those of conventional concrete box girder sections or solid sections. Therefore, at the same

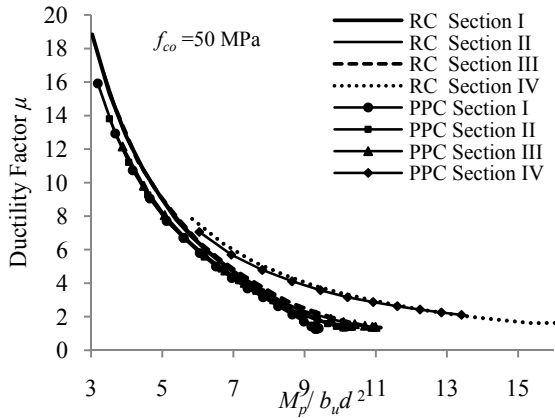


Fig. 15 Flexural strength - ductility performance at same overall dimensions

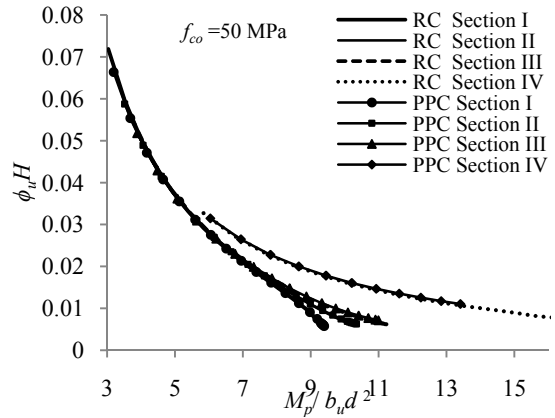


Fig. 16 Flexural strength - deformability performance at same overall dimensions

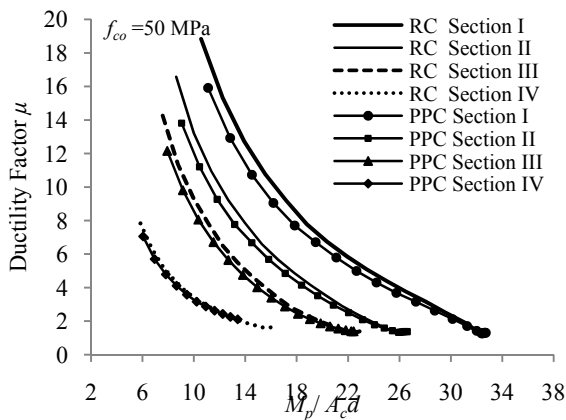


Fig. 17 Flexural strength - ductility performance at same concrete area

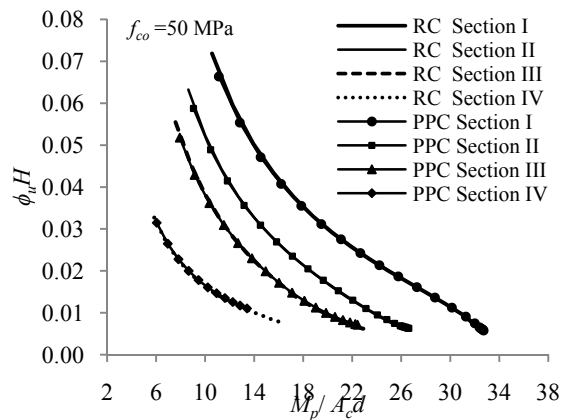


Fig. 18 Flexural strength - deformability performance at same concrete area

overall dimensions, the flexural strength - ductility and flexural strength - deformability performance of Section I with corrugated steel webs is inferior to that of conventional concrete box girder sections or solid sections.

The above comparison is based on the premise that all the sections analysed have the same overall dimensions. To be fair, comparison should be carried out for the same concrete sectional area in view of its large variation among sections. To study the performance at the same concrete sectional area, the ductility factors and deformability indicators are plotted against $M_p/A_c d$, where A_c is the concrete sectional area above the centroid of the tension steel reinforcement.

Fig. 17 and 18 show the flexural strength - ductility and flexural strength - deformability performance, respectively, of sections having the same section concrete area. Obviously, at the same concrete sectional area, the flexural strength - ductility and flexural strength - deformability performance of Section I with corrugated steel webs is much better than that of Sections II and III of conventional concrete box girder construction or Section IV of solid construction.

Taking into account the self-weight, the RC and PPC sections with corrugated steel webs

provide the best flexural strength - ductility and flexural strength - deformability performance.

4. Effects of interaction between shear deformation and local bending of flanges

The interaction between shear deformation and local bending of concrete flanges may cause secondary bending moment M_2 and secondary shear force V_2 to be resisted by the pair of concrete flanges and hence stress concentration in the concrete flanges, especially in the vicinities of the point load and diaphragm (Chen *et al.* 2015b).

For example, the loaded section of a simply supported bridge under a vertical point load F at mid-span as shown in Fig. 19 is considered. By symmetry, only analysis of the right half is carried out with the origin taken at mid-span. According to the extended sandwich beam model proposed by Chen *et al.* (2015b), the secondary bending moment M_2 and secondary shear force V_2 due to the interaction between shear deformation and local bending of concrete flanges are solved as

$$M_2 = [F/(2\alpha)] [\tanh(\alpha l) \cosh(\alpha x) - \sinh(\alpha x)] \quad (4)$$

$$V_2 = -(F/2) [\cosh(\alpha x) - \tanh(\alpha l) \sinh(\alpha x)] \quad (5)$$

where $\alpha = \sqrt{(\beta^2 S_w / B_f)(B/B_g)}$; B_f is the sum of the local bending stiffnesses of the flanges about their respective centroidal axes; B_g is the global bending stiffness of the flanges about the centroidal axis of the entire beam assuming uniform stress in each flange; B is the total flexural rigidity; β is equal to h / h_w as shown in Fig. 1; S_w is the equivalent shear rigidity of the corrugated steel webs; and l is the distance from the point load F to the right support. The value of $\tanh(\alpha l)$ in Eqs. (4) and (5) increases exponentially to approximately unity at values of αl at about 5. With $\tanh(\alpha l)=1$, Eqs. (4) and (5) become

$$M_2 = [F/(2\alpha)] e^{-|\alpha x|} \quad (6)$$

$$V_2 = -(F/2) e^{-|\alpha x|} \quad (7)$$

which indicate that the secondary bending moment M_2 and secondary shear force V_2 diminish exponentially to almost zero at distance $x \geq 5/\alpha$ along the bridge in accordance with the exponential function as shown in Fig. 20. From Eqs. (6) and (7), the secondary bending moment M_2 and secondary shear force V_2 due to interaction effects reach the peak values $M_{2,peak}=F/(2\alpha)$ and $M_{2,peak}=-F/2$, respectively, at mid-span.

The secondary curvature ϕ_2 of the concrete flanges caused by the interaction effects is obtained as

$$\phi_2 = M_2 / B_f \quad (8)$$

The secondary bending moment M_2 and secondary shear force V_2 are carried by the pair of concrete flanges. To consider the interaction effects in section analysis, the secondary curvature ϕ_2 associated with additional local bending induced in the concrete flanges is determined upon application of the primary curvature ϕ_1 to the entire section as shown in Fig. 21, in which the values of α and B_f are updated accordingly to account for material nonlinearity as necessary.

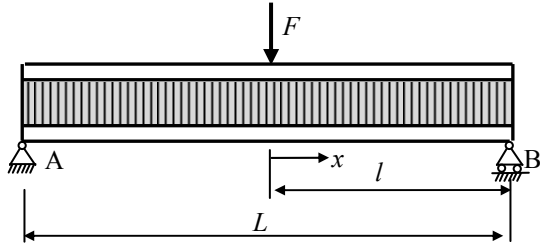


Fig. 19 A simply-supported bridge under a vertical point load F at mid-span

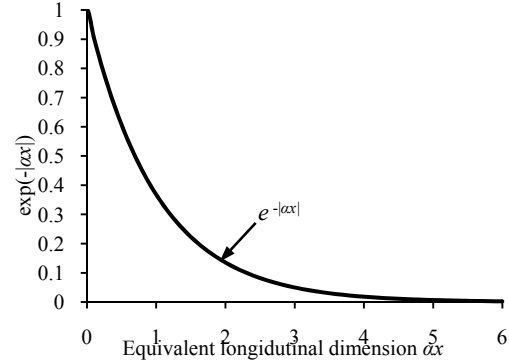


Fig. 20 Exponential function of dissipation

For beam sections with significant interaction effects, possible shear failure of concrete flanges should be taken into account. Shitou *et al.* (2008) carried out shear tests on full- and half-scale models and found that the contribution of corrugated steel web to shear increased with the propagation of cracking of concrete flanges. In this study when the shear force carried by a concrete flange reaches its strength, the concrete flange is assumed to fail immediately due to its brittle character (Inel and Ozmen 2006) and the corrugated steel webs then carry the additional shear force. After shear failure of the concrete flanges, the secondary curvature ϕ_2 still continues to develop to meet the local compatibility requirement. The zone with significant secondary effects may form a local plastic hinge, which is closely related to the exponential dissipation of the concentrated secondary bending moment M_2 and shear force V_2 . The equivalent length l_{ps} of local plastic hinge, over which the secondary curvature ϕ_2 is considered to be constant at the peak value, can be estimated by equating the hypothetical rectangular area of the plastic hinge to the actual area of secondary curvature distribution. When the bridge remains elastic and hence the parameter α is a constant, the equivalent length l_{ps} can be obtained as $l_{ps} \approx 2/\alpha$ based on properties of the function in Fig. 20, which reflects the secondary bending moment on one side of the plastic hinge. In the plastic stage when the parameter α varies along the length of local plastic hinge due to material nonlinearity, a trial and error process is needed for determination of l_{ps} .

A section with corrugated steel webs at the mid-span of a simply supported bridge of span $L=30$ m with cross-sectional dimensions as shown in Fig. 8 is analysed. The tension steel area A_s and compression steel A'_s are assumed to be 0.15 m^2 and 0.05 m^2 respectively and evenly distributed in two layers of each flange. Each layer of steel is at 70 mm from its nearest horizontal concrete surface. The in-situ concrete compression strength f_{co} , the yield strength of non-prestressed reinforcement and the yield strength of corrugated steel webs are 50 MPa, 500 MPa, and 400 MPa respectively. The Young's modulus of both non-prestressed reinforcement and corrugated steel webs are 200 GPa. The thickness of corrugated steel webs is 20 mm. The complete moment-curvature curves of the mid-span section considering interaction effects are obtained and compared with that ignoring interaction effects as shown in Fig. 22, which shows that interaction has little effect on the ultimate curvature and deformability, but significantly increases the yield curvature and decreases the ductility. The total curvature ϕ considering interaction effects is found to reverse when the resisting moment M drops significantly, i.e., "snap back" phenomenon. It is because the secondary curvature ϕ_2 decreases with the drop of resisting shear force V and bending

moment M . However, this should be treated with caution, as the upper concrete flange may be crushed thereby creating a kink and violating the assumptions made in the numerical model. However, the effects of curvature reversal on strength, ductility and deformability of the section are insignificant.

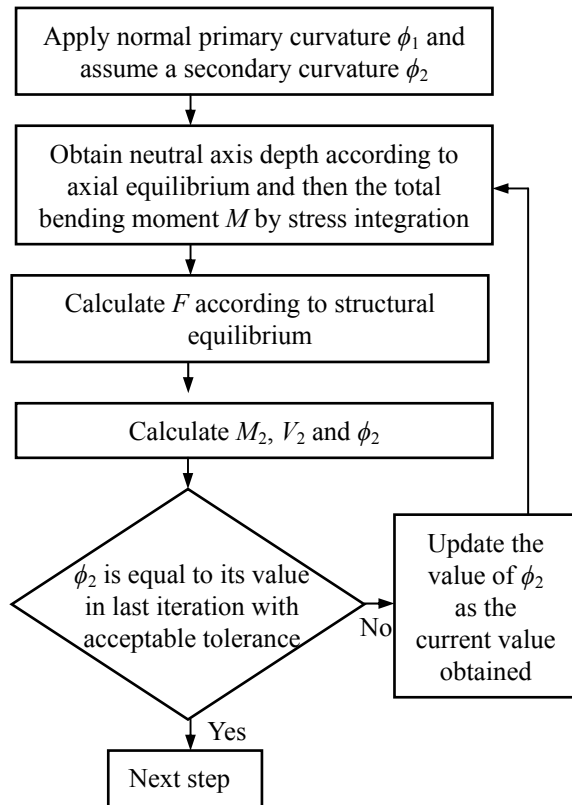


Fig. 21 Flow chart of section analysis considering interaction effects

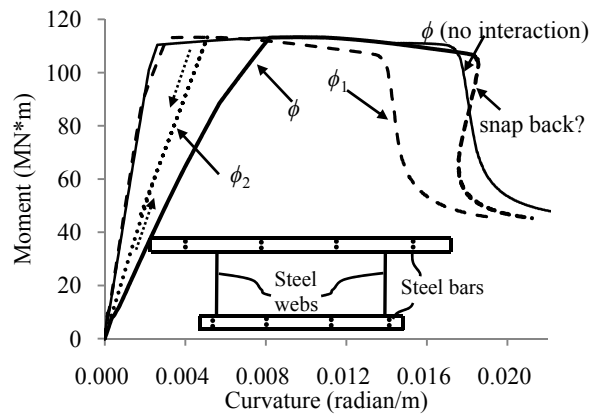


Fig. 22 Complete moment-curvature curves considering interaction effects

The strain distributions over section depth at different stages as shown in Fig. 23 indicate that the interaction effects decrease as the primary curvature ϕ_1 increases. Firstly, as the primary curvature ϕ_1 increases, the local flexural stiffness B_f decreases due to material nonlinearity and therefore the parameter α increases. Secondly, after the yielding of steel, the primary curvature continues to increase, while the resisting moment remains roughly the same. Therefore the resisting shear force and associated secondary curvature ϕ_2 only vary a bit, causing the ratio of secondary curvature to total curvature to decrease. As the interaction effects are quite localized, it is difficult to verify these effects by tests. However, the zigzag distribution of normal strain over section depth has been observed in some tests, e.g., Ikeda *et al.* (2002), Kadotani *et al.* (2002), Chen *et al.* (2015b).

The interaction effects are sensitive to the span L and the parameter α . Fig. 24 shows that, as the span L decreases, the yield curvature increases thereby reducing the ductility. With a shorter

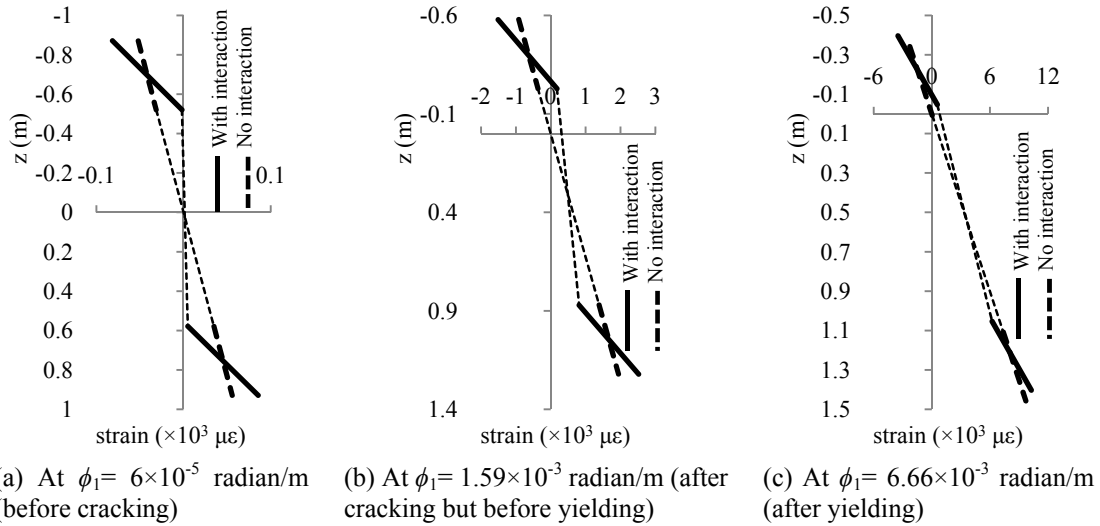


Fig. 23 Strain distributions over section depth

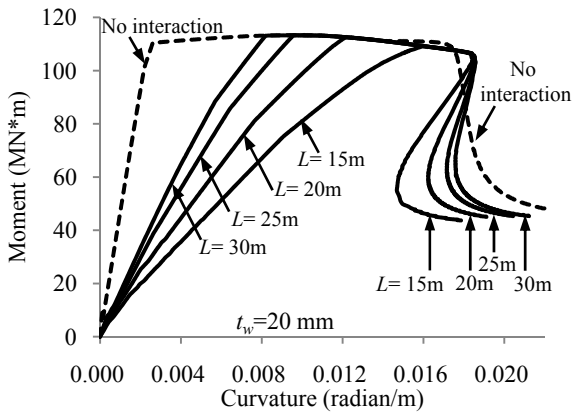


Fig. 24 Effect of span L on interaction

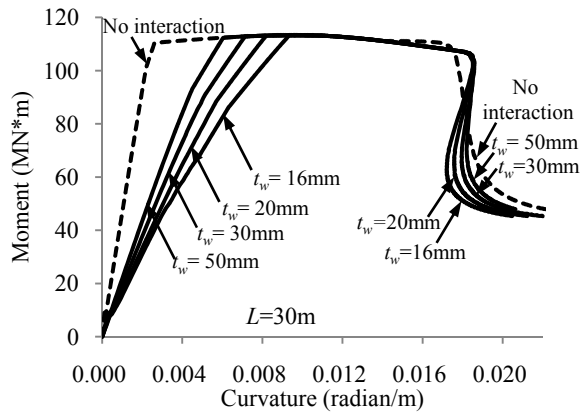


Fig. 25 Effects of total thickness of corrugated steel webs on interaction

span L , the dominant shear causes significant interaction effects between shear deformation and local bending of concrete flanges. The parameter α is approximately equal to the square root of the ratio of the equivalent shear rigidity $\beta^2 S_w$ of the entire section to the local bending stiffness B_f of concrete flanges. For convenience, the parameter α is varied by changing the total thickness of corrugated steel webs. Fig. 23 shows that, with the reduction of total thickness t_w of corrugated steel webs, the yield curvature increases, which reduces the ductility. As the total thickness t_w and parameter α reduce, the larger shear deformation causes more significant interaction effects. Any other changes causing variation in parameter α , e.g. local bending stiffness B_f , will also affect the interaction effects.

5. Conclusions

The ductility, deformability and strength of RC and PPC sections with corrugated steel webs are studied and compared with those of conventional sections. The analysis considers the equilibrium of section, and the actual stress-strain curves of materials with possible strain reversal. The interaction effects between shear deformation and local bending of concrete flanges are studied by considering the secondary curvature in concrete flanges. The numerical results also agree well with experimental results.

The following conclusions can be drawn: (a) Concrete bridges with corrugated steel webs perform reasonably well in respect of flexural ductility and deformability; (b) In comparison with concrete box girder sections and solid concrete sections, concrete bridges with corrugated steel webs still perform well in respect of flexural ductility and deformability provided that those with the same concrete sectional areas are compared; (c) The effects of prestressing force ratio on the deformability indicator are insignificant; (d) Increase in PPR tends to adversely affect the ductility factor and deformability indicator; (e) The interaction effects between shear deformation and local bending of concrete flanges are sensitive to the arrangement of span and loading, and sectional properties; and (f) The interaction effects on ultimate curvature and deformability are insignificant.

Acknowledgements

The work reported in this paper is supported by the Research Grants Council (RGC) of the Hong Kong Special Administrative Region, China (RGC Project No. HKU 710111E).

References

- Attard, M.M. and Setunge, S. (1996), "The stress-strain relationship of confined and unconfined concrete", *ACI Mater. J.*, **93**(5), 432-442.
- Attard, M.M. and Stewart, M.G. (1998), "A two parameter stress block for high-strength concrete", *ACI Struct. J.*, **95**(3), 305-317.
- Au, F.T.K., Leung, C.C.Y. and Kwan, A.K.H. (2011), "Flexural ductility and deformability of reinforced and prestressed concrete sections", *Comput. Concrete*, **8**(4), 473-489.
- Bai, Z.Z. and Au, F.T.K. (2013), "Flexural ductility design of high-strength concrete beams", *Struct. Des. Tall Spec.*, **22**, 521-542.
- Barros, H.F.M. and Martins, R.A.F. (2012), "Nonlinear analysis of service stresses in reinforced concrete sections - closed form solutions", *Comput. Concrete*, **10**(5), 541-555.
- Briassoulis, D. (1986), "Equivalent orthotropic properties of corrugated sheets", *Comput. Struct.*, **23**(2), 129-138.
- Carreira, D.J. and Chu, K.H. (1986), "The moment-curvature relationship of reinforced concrete members", *ACI Struct. J.*, **95**, 725-739.
- Chen, X., Zhou, D.H., Wang, P. and Zhang, S.P. (2015a), "New procedure for determining the moment-curvature relationship of a reinforced concrete section", *Mag. Concrete Res.*, **67**(3), 121-132.
- Chen, X.C., Bai, Z.Z., Au, F.T.K. and Zeng, Y. (2015b), "An extended sandwich theory for prestressed concrete bridges with corrugated steel web(s)", *Report of IABSE Conference on "Elegance in Structures"*, Nara, Japan, June.
- Cheyrezy, M. and Combault, J. (1990), "Composite bridges with corrugated steel webs - achievements and prospects", *IABSE Symposium on Mixed Structures including New Materials*, Brussels, Belgium,

September.

- Cohn, M.Z. and Riva, P. (1991), "Flexural ductility of structural concrete sections", *PCI J.*, **36**(2), 72-87.
- Elmorsi, M., Kianoush, M.R. and Tso, W.K. (1998), "Nonlinear analysis of cyclically loaded reinforced concrete structures", *ACI Struct. J.*, **95**, 725-739.
- Guo, Z.H. and Zhang, X.Q. (1987), "Investigation of complete stress-deformation curves for concrete in tension", *ACI Mater. J.*, **84**(4), 278-285.
- Havaei, G.R. and Keramati, A. (2011), "Experimental and numerical evaluation of the strength and ductility of regular and cross spirally circular reinforced concrete columns for tall buildings under eccentric loading", *Struct. Des. Tall Spec.*, **20**(2), 247-256.
- Ho, J.C.M., Kwan, A.K.H. and Pam H.J. (2003), "Theoretical analysis of post-peak flexural behaviour of normal- and high-strength concrete beams", *Struct. Des. Tall Spec.*, **12**, 109-125.
- Ikeda, H., Ashiduka, K., Ichinomiya, T., Okimi, Y., Yamamoto, T. and Kano, M. (2002), "A study on design method of shear buckling and bending moment for prestressed concrete bridges with corrugated steel webs", *Session 5: Composite structures, Proceedings of the 1st fib Congress*, Osaka, Japan, October.
- Inel, M. and Ozmen, H.B. (2006), "Effects of plastic hinge properties in nonlinear analysis of reinforced concrete buildings", *Eng. Struct.*, **28**, 1494-1502.
- Kadotani, T., Aoki, K., Ashizuka, K., Mori, T., Tomimoto, M. and Kano, M. (2002), "Shear buckling behavior of prestressed concrete girders with corrugated steel webs", *Session 5: Composite structures, Proceedings of the 1st fib Congress*, Osaka, Japan, October.
- Kwan, A.K.H. and Au, F.T.K. (2004), "Flexural strength-ductility performance of flanged beam sections cast of high-strength concrete", *Struct. Des. Tall Spec.*, **13**, 29-43.
- Lee, H.J. (2013), "Predictions of curvature ductility factor of doubly reinforced concrete beams with high strength materials", *Comput. Concrete*, **12**(6), 831-850.
- Mander, J.B., Priestley, M.J.N. and Park, R. (1984), "Seismic design of bridge piers", Research Report 84-2, Department of Civil Engineering, University of Canterbury, Christchurch.
- Menegotto, M. and Pinto, P.E. (1973), "Method of analysis for cyclically loaded R.C. plane frames", *IABSE Preliminary Report for Symposium on Resistance and Ultimate Deformability of Structures Acted on by Well Defined Repeated Loads*, Lisbon, Portugal.
- Naaman, A.E. (1985), "Partially prestressed concrete: review and recommendations", *PCI J.*, **30**(6), 31-71.
- Naaman, A.E., Harajli, M.H. and Wight, J.K. (1986), "Analysis of ductility in partially prestressed concrete flexural members", *PCI J.*, **31**(3), 64-87.
- Pandey, A.K. (2013), "Flexural ductility of RC beam sections at high strain rates", *Comput. Concrete*, **12**(4), 537-552.
- Park, R. (1988), "Ductility evaluation from laboratory and analytical testing", *Proceedings of the 9th World Conference on Earthquake Engineering, VIII*, Kyoto, Japan, August.
- Samanta, A. and Mukhopadhyay, M. (1999), "Finite element static and dynamic analysis of folded plates", *Eng. Struct.*, **21**(3), 277-287.
- Shitou, K., Nakazono, A., Suzuki, N., Nagamoto, N. and Asai, H. (2008), "Experimental research on shear behavior of corrugated steel web bridge", *JSCE, Divison A*, **64**(2), 223-234. (in Japanese)
- Thompson, K.J. and Park, R. (1980), "Ductility of prestressed and partially prestressed concrete beam sections", *PCI J.*, **25**(2), 46-70.
- Whitehead, P.A. and Ibell, T.J. (2004), "Deformability and ductility in over-reinforced concrete structures", *Mag. Concrete Res.*, **56**(3), 167-177.